The study of the valence-shell excitations of chlorotrifluoromethane by fast electron impact

Jin-Feng Chen[1], Jian-Hui Zhu[1], Muhammad Meesum Bilal[1] ,
En-Chao Huang[1], and Lin-Fan Zhu[1,*]
[1]Hefei National Research Center for Physical Sciences at Microscale and Department of Modern Physics, University of Science and Technology of China, Hefei, Anhui 230026, China

September 17, 2026

Abstract

The oscillator strengths and cross sections of the valence-shell excitations in chlorotrifluoromethane (CF_3Cl) are highly important for understanding atmospheric evolution and modeling plasma etching. In this work, absolute generalized oscillator strengths (GOSs) for these excitations were measured by an angle-resolved electron energy loss spectrometer operating at a collision energy of 1500 eV and an energy resolution of approximately 120 meV. By extrapolating the GOSs to zero momentum transfer, the optical oscillator strengths (OOSs) were determined. In addition, using the BE-scaling method, the integral cross sections (ICSs) for the corresponding excitations were calculated from the threshold energies up to 5000 eV. The presently obtained data provide an independent verification of the previous findings and contribute to the fundamental molecular database of CF_3Cl. The datasets presented in this paper, including the GOSs, OOSs and ICSs, are openly available at https://doi.org/10.57760/sciencedb.j00113.00346 (https://www.scidb.cn/s/Uz26Fb).

Keywords: chlorotrifluoromethane, electron scattering, oscillator strength, integral cross section
PACS: 34.80.Gs, 33.70.Ca

1. Introduction

Chlorotrifluoromethane (CF_3Cl) serves as a key industrial material in applications such as refrigerant, aerosol propellant, and etchant [1–5]. Because of its high ozone-depletion and global-warming potential, the Montreal Protocol has mandated the phase-out of CF_3Cl's production and use [6]. Nevertheless, the atmospheric lifetime of CF_3Cl is relatively long (approximately 640 years), which means it remains a great source of environmental concern [7].

The energy level structures of the valence-shell excitations of CF_3Cl have been widely investigated by photoabsorption methods [8–16], electron impact methods [17–21] and theoretical calculations [3, 22–24]. Among

*Corresponding author. E-mail: lfzhu@ustc.edu.cn

them, the photoabsorption cross sections, or equivalent optical oscillator strength densities (OOSDs), were early measured with the photoabsorption methods in limited wavelength (energy) regions [8–16]. With the development of dipole (e,e) method, i.e., the electron energy loss spectroscopy (EELS) conducted at a scattering angle of $\sim 0^\circ$, the measurements of OOSDs were extended to larger energy regions up to several hundred eV [17, 18, 21]. Note that the low-resolution measurements of Zhang *et al.* [18] suffered from large background subtraction errors, which were later corrected by Au *et al.* [21]. As for the state-resolved optical oscillator strength (OOS), the only experimental data were reported for the first excited singlet-state of CF_3Cl, which were obtained by extrapolating the EELS-measured generalized oscillator strengths (GOSs) to zero momentum transfer [19, 20]. In theory, the OOSs of the first several excited singlet-states were calculated using methods including multi-reference configuration interaction with single and double excitations (MR-CISD) [6, 25, 26] and equation-of-motion coupled-cluster singles and doubles (EOM-CCSD) [27].

Regarding the GOS, Ying and Leung [19] and Ying *et al.* [20] obtained the GOSs for transitions at 7.7, 9.6, 10.6 and 11.5 eV by an angle-resolved EEL spectrometer operated at a collision energy of 2.5 keV. However, the low energy resolution of 0.8 eV in their experiment [19, 20] can not clearly separate the adjacent transitions, which may lead to large GOS uncertainties due to the random intensity allocations in their fitting procedure. Similar phenomena have been noticed in the GOSs measurements of CF_4 [28], CHF_3 [29], CCl_4 [30] and $CFCl_3$ [31]. Theoretically, only the GOSs of the excited states of 1 ^{1}E and 2 ^{1}E of CF_3Cl were calculated by Watanabe and Takahashi using the EOM-CCSD method [27]. With respect to the integral cross sections (ICSs) for the electron impact valence-shell excitations of CF_3Cl, although they are essential input parameters for relevant plasma etching modeling [5], to our knowledge, no experimental or theoretical results have been reported previously.

To address the aforementioned limitations in the previous studies, an improved measurement of the GOS, OOS, and ICS data of CF_3Cl is required. In the present work, employing the angle-resolved EELS method, we determined the GOSs of the valence-shell excitations of CF_3Cl, and derived the associated OOSs and ICSs. The higher resolution achieved in this work reduced the fitting errors compared to the previous studies, thereby improving the accuracy of the measured data. In the following, the experimental methodology, fitting procedure, and data analysis are outlined in Section 2. Section 3 presents and discusses the experimental results. Finally, a summary of this work is given in Section 4.

2. Experimental methods

A high-resolution fast EEL spectrometer was used to measure the GOSs for CF_3Cl, which has been detailed in our early studies [32–34]. In the experiment, the incident electron energy was set at 1500 eV and the instrumental resolution was approximately 120 meV. To improve measurement accuracy and simplify normalization process, the relative flow technique was employed [35–37]. During the experiment, CF_3Cl gas and standard helium gas were mixed at controlled flow rates and introduced continuously into an interaction chamber, where it crossed the incident electron beam at 90°. The pressures in the interaction chamber with and without the mixed gas were about 3×10^{-3} and 5×10^{-5} Pa, respectively. The physical 0° was calibrated with the inelastic scattering signals of He: $1s^2\ ^1S_0 \rightarrow 1s2p\ ^1P_1$ around the geometrical 0°, and the instrumental energy resolution was determined as the full width at half maximum (FWHM) of the spectral feature of the same transition.

Comparisons of data at different flow rates confirmed that the present results were free from the pressure effect [33, 38]. The EEL spectra at scattering angles of 1°-8° were recorded, corresponding to $K^2 \approx 0.04$ - 2.15 a.u..

For a discrete transition, the GOS is defined as:

$$f(\boldsymbol{K}, E_n) = \frac{2E_n}{K^2} \left| \langle \Psi_n | \sum_{j=1}^{N} e^{i\mathbf{K}\cdot\mathbf{r}_j} | \Psi_0 \rangle \right|^2 . \tag{1}$$

Here E_n and $\boldsymbol{K}$ are the excitation energy and momentum transfer, respectively. $\mathbf{r}_j$ is the position of the j-th electron, and Ψ_0 and Ψ_n denote the initial- and final-state N-electron wave-functions. Within the first Born approximation (FBA) [39], the GOS and the differential cross section (DCS) $\frac{d\sigma}{d\Omega}$ are interconvertible:

$$f(\boldsymbol{K}, E_n) = \frac{E_n}{2} \frac{p_0}{p_a} K^2 \frac{d\sigma}{d\Omega}, \tag{2}$$

where p_0 and p_a represent the magnitudes of the electron momenta before and after scattering. Owing to relative flow technique, the measured DCSs for the excitations of CF_3Cl can be normalized to an absolute scale via

$$\frac{d\sigma^{\mathrm{T}}(E_n, \theta)}{d\Omega} = \frac{d\sigma^{\mathrm{S}}(E'_n, \theta)}{d\Omega} \frac{N^{\mathrm{T}}(E_n, \theta)}{N^{\mathrm{S}}(E'_n, \theta)} \frac{\dot{n}^{\mathrm{S}}}{\dot{n}^{\mathrm{T}}} \frac{\sqrt{M^{\mathrm{S}}}}{\sqrt{M^{\mathrm{T}}}}, \tag{3}$$

where the superscripts T and S represent the CF_3Cl and He, respectively. $N^{\mathrm{T}}(E_n, \theta)$ and $N^{\mathrm{S}}(E'_n, \theta)$ are the counts of scattered electrons for CF_3Cl and He, where E_n and E'_n are the respective excitation energies and θ is the scattering angle. $\dot{n}$ and M denote the corresponding flow rate and atomic (or molecular) mass. According to Eqs. (2) and (3), the GOSs of CF_3Cl were attained through normalizing the measured data to the one of He: $1s^2\ {}^1S_0 \rightarrow 1s2p\ {}^1P_1$, which holds a high accuracy both experimentally and theoretically [33, 40–42].

The normalized GOSs were expanded using the Lassettre formula[43–45]:

$$f(\boldsymbol{K}, E_n) = \frac{1}{(1+x)^6} \sum_{m=0}^{\infty} \frac{f_m x^m}{(1+x)^m}. \tag{4}$$

Here $x = K^2/\alpha^2$, with α^2 being a fitting factor. f_m is the fitting parameter, where f_0 corresponds to the OOS. An exponential function with extra fitting parameters b and c may be added to Eq. (4) to account for the possible second maximum in the GOS:

$$g(x) = bx \cdot e^{-cx}. \tag{5}$$

CF_3Cl belongs to the C_{3v} molecular point group, where its valence-shell electronic configuration is described as [19, 27]

$$(\mathrm{core})^{18}(6a_1)^2(3e)^4(7a_1)^2(8a_1)^2(4e)^4(9a_1)^2(5e)^4(6e)^4(1a_2)^2(10a_1)^2(7e)^4 : {}^1A_1.$$

The EEL spectra of CF_3Cl measured at 1.0° and 4.5° are plotted in Figs. 1(a) and 1(b) respectively, and the measured GOS density is visualized as a two-dimensional map in Fig. 1(c). In line with Refs. [17, 19], the valence-shell excitations of CF_3Cl include $7e \rightarrow 11a_1$ at 7.7 eV, $7e \rightarrow 4s$ at 9.6 eV, $7e \rightarrow 4p$ at 10.6 eV and $7e \rightarrow 5s, 3d$ at 11.5 eV, as illustrated in Fig. 1(b). To accurately determine the scattering intensities of these transitions, a least-squares fit was performed on the measured spectra. Figs. 1(a) and 1(b) clearly demonstrate that $7e \rightarrow 11a_1$ has a dipole-forbidden character, i.e., a quite low intensity at small squared momentum transfer while a high intensity at large momentum transfer. In contrast, other transitions are typical dipole-allowed transitions. Therefore, when performing the fitting, the peak positions and profiles of $7e \rightarrow 4s$, $7e \rightarrow 4p$ and

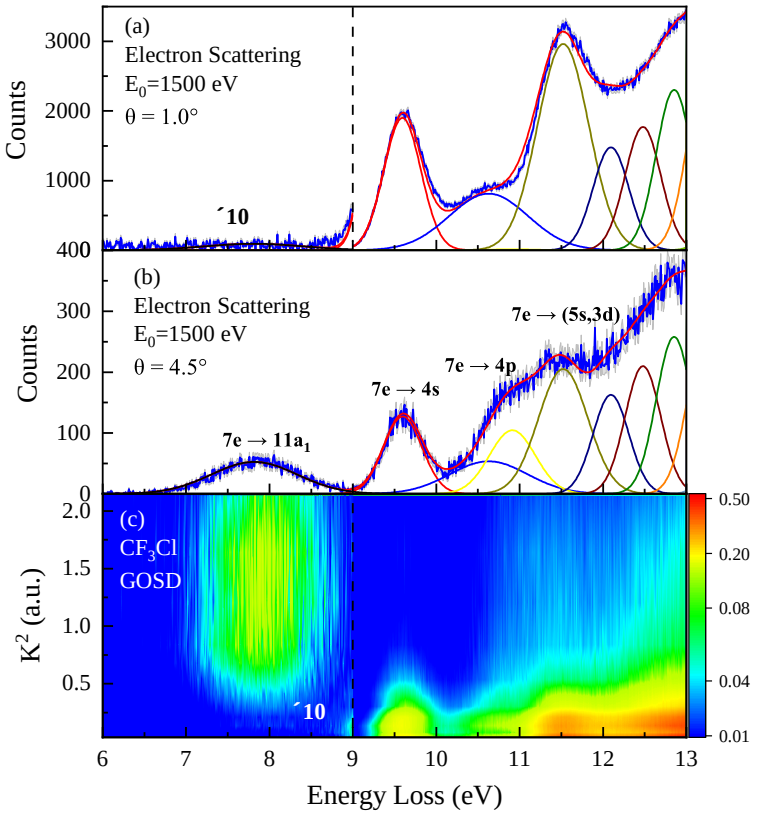


Figure 1: The EELS spectra of the valence-shell excitations of CF_3Cl measured at (a) 1.0° and (b) 4.5°. The gray shaded area indicates the statistical errors of the experimental data. The fitted results are also presented with the transition assignments labeled. (c) A two-dimensional GOS density map of CF_3Cl.

$7e \rightarrow 5s, 3d$ were fixed to their average values at small angles (1.0°-3.5°), which were obtained by preliminarily fitting the spectra measured at 1.0°-3.5° with Gaussian functions. Furthermore, to reproduce the observed spectra well, an additional Gaussian curve at 10.9 eV was added to depict the feature of $7e \rightarrow 4p$, as shown in Fig. 1 (b). As for the first transition of $7e \rightarrow 11a_1$, Pearson IV function that reproduces this feature well was used, with fixed energy position and peak profile obtained by averaging the preliminary fitted results at large angles (4.0°-8.0°).

The errors associated with the measured GOSs can be attributed to five main sources: the statistical counting, fitting procedure, angular resolution, angle determination, and normalization method. The total experimental uncertainties, obtained by calculating the root sum of squares of these contributions, are typically in the range of 10%–15%.

3. Results and discussion

Table 1: The present experimental GOSs and extrapolated OOSs of the valence-shell excitations of CF_3Cl. The data have been multiplied by 10^3, and the numbers in parentheses are the experimental uncertainties.

K^2(a.u.)	$7e \rightarrow 11a_1$	$7e \rightarrow 4s$	$7e \rightarrow 4p$	$7e \rightarrow 5s, 3d$
0(OOS)	0.2(0.2)	149.6(14.9)	122.9(13.2)	330.0(30.5)
0.04	1.2(1.3)	114.6(11.5)	117.5(11.7)	301.7(30.2)
0.08	1.7(0.9)	109.2(10.9)	114.1(11.4)	286.6(28.7)
0.14	2.0(0.5)	92.0(9.2)	103.3(10.3)	223.6(22.4)
0.22	2.4(0.3)	74.1(7.4)	85.7(8.6)	179.5(17.9)
0.31	3.4(0.3)	47.2(4.7)	54.7(5.5)	103.5(10.4)
0.41	4.9(0.5)	34.5(3.4)	44.8(4.5)	69.4(6.9)
0.53	6.9(0.7)	20.5(2.0)	31.4(3.1)	42.1(4.2)
0.66	10.0(1.0)	13.4(1.3)	27.2(2.7)	33.4(3.3)
0.83	11.5(1.1)	7.6(0.8)	22.2(2.2)	26.5(2.6)
1.21	12.2(1.2)	4.9(0.5)	18.0(1.8)	23.2(2.3)
1.65	12.4(1.2)	5.3(0.5)	17.0(1.7)	20.2(2.0)
2.15	8.4(0.9)	4.7(0.5)	12.8(1.3)	15.7(1.6)

The measured GOSs of CF_3Cl are numerically listed in Table 1 and plotted in Figs. 2-6. Fig. 2 displays the GOS of $7e \rightarrow 11a_1$ at 7.9 eV along with the previous measurement at 2.5 keV [19] and EOM-CCSD calculation [27]. Fig. 2 clearly shows the typical dipole-forbidden GOS behavior, i.e., it exhibits a near-zero value at $K^2 \approx 0$, followed by a gradual increase in the small K^2 regime, reaching its maximum at roughly 1.6 a.u., after which it decreases with further increasing K^2. The above behavior characterizes the dipole-forbidden nature of $7e \rightarrow 11a_1$. The theoretical GOSs [27] calculated with and without the vibronic effect show minor difference, as exhibited in Fig. 1 in Ref. [27], so only the one with vibronic effect is given in Fig. 2. It is clear that the theoretical GOS has a similar profile to the present result, while it is somewhat larger when $K^2 > 0.2$ a.u.. Similarly, the previously measured GOS [19] has a similar profile with the present one, while its magnitudes are

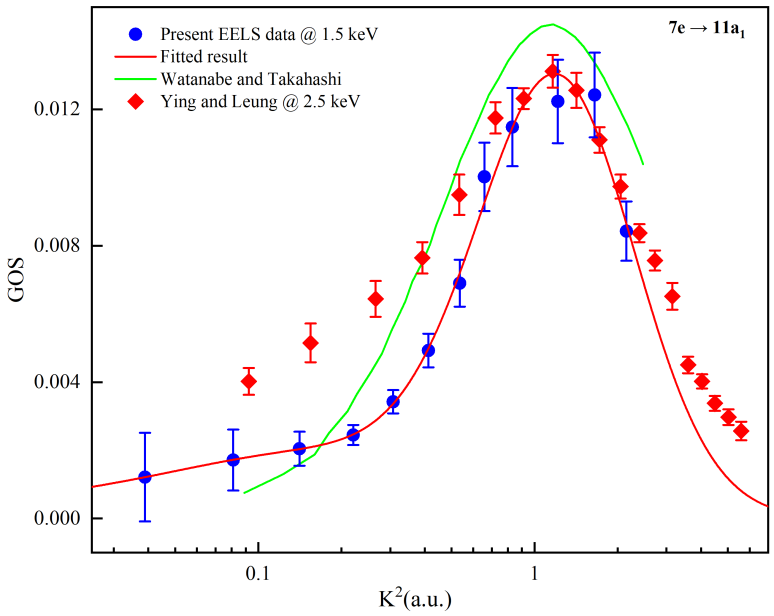


Figure 2: The GOS for the transition $7e \rightarrow 11a_1$ of CF_3Cl in comparison with the measurement of Ying and Leung [19] and theoretical calculation of Watanabe and Takahashi [27].

higher in small K^2. This discrepancy may likely originate from the random intensity allocation in their fitting process, given that the weak intensity of $7e \rightarrow 11a_1$ in small K^2 and the limited energy resolution (0.8 eV).

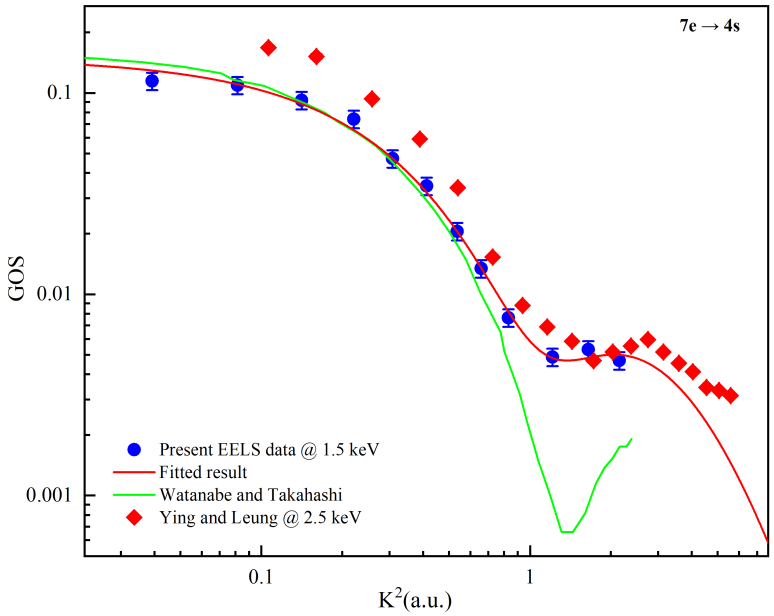


Figure 3: Same as Fig. 2, but for the $7e \rightarrow 4s$ transition.

Fig. 3 presents our GOS of $7e \rightarrow 4s$ transition at 9.6 eV and the ones available in literature [19, 27], and all of them exhibit similar dipole-allowed profiles, i.e., decreasing quickly as K^2 increases in the small K^2 region. It is clear that the theoretical result [27] is highly consistent with the present one when $K^2 < 0.8$ a.u., yet it is lower at $K^2 > 0.8$ a.u.. As for the experimental GOS of Ying and Leung [19], it is generally higher than the present one.

The present GOS for $7e \rightarrow 4p$ transition at 10.6 eV along with the previous experimental result [19] is

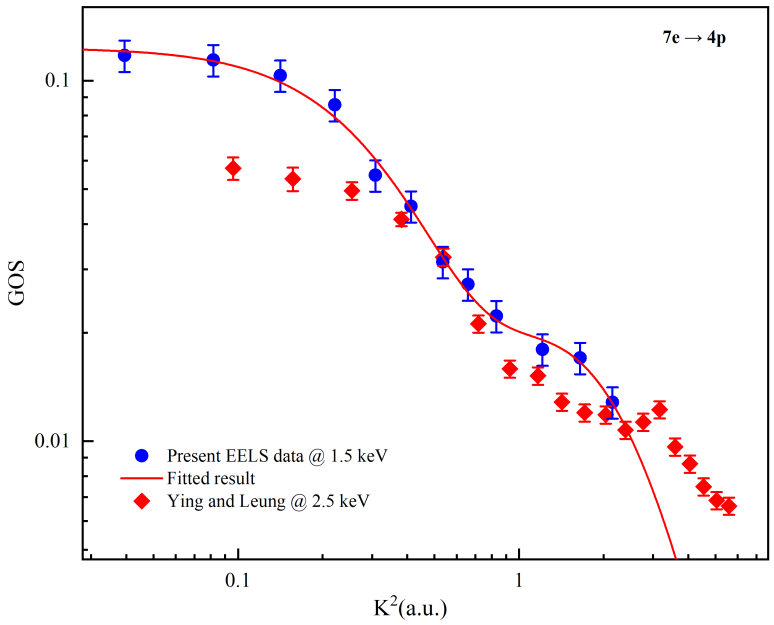


Figure 4: Same as Fig. 2, but for the $7e \rightarrow 4p$ transition.

shown in Fig. 4. It is found that the previous experimental result [19] is significantly lower than the present one when $K^2 < 0.3$ a.u. and $K^2 > 0.7$ a.u.. To elucidate the GOS differences between this study and Ref. [19] that are displayed in Figs. 3 and 4, the overall GOSs of $7e \rightarrow 4s$ and $7e \rightarrow 4p$ are plotted in Fig. 5, which can reduce the fitting errors originated from the different energy resolution. It is obvious in Fig. 5 that the total GOSs measured by this work and Ref. [19] show very good consistency in whole K^2 regime. This result clearly demonstrates the advantage of our high-resolution measurement. Under low energy resolution conditions, the instrumental broadening effect significantly smears out adjacent transition features, making it difficult to resolve individual peaks that are closely spaced in the experimental spectra. In this scenario, the fitting procedure can not unambiguously identify the exact contribution of each independent transition component, which introduces considerable fitting errors. As a result, the apparent peak intensities tend to be randomly distributed among overlapping transitions during the fitting process. Although the total intensity of the entire spectral envelope can still be determined with relatively high accuracy, the extracted intensity of each individual transition peak deviates substantially from its true value. In contrast, when the measurement is performed at sufficiently high energy resolution, the fine spectral structures corresponding to different transitions can be more clearly separated and directly distinguished in the experimental spectra. In this case, the ambiguity in peak intensity allocation is largely eliminated. The corresponding fitting error for each independent peak is thus remarkably reduced, and the retrieved intensity of each individual transition can be determined with much higher precision. Therefore, the discrepancies shown in Figs. 3 and 4 can be largely attributed to the fitting error in Ref. [19] due to their low resolution of 0.8 eV. Furthermore, the good agreement of the GOSs measured at 1.5 and 2.5 keV implies that the FBA is applicable at a collision energy of 1.5 keV for the excitations of $7e \rightarrow 4s$ and $7e \rightarrow 4p$ of CF_3Cl.

The last feature at 11.5 eV is attributed to the $7e \rightarrow 5s, 3d$ transition, which is dipole-allowed. The present experimental GOS for this transition is compared with the previous one [19] in Fig. 6. Obviously, the two results have similar profile although the previous data [19] is slightly larger in small K^2 region.

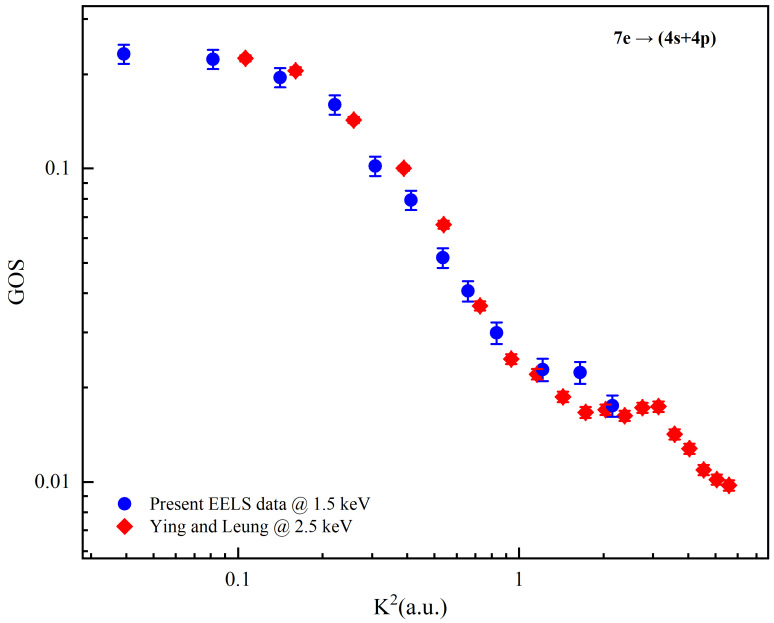


Figure 5: Same as Fig. 2, but for the $7e \rightarrow (4s + 4p)$ transitions.

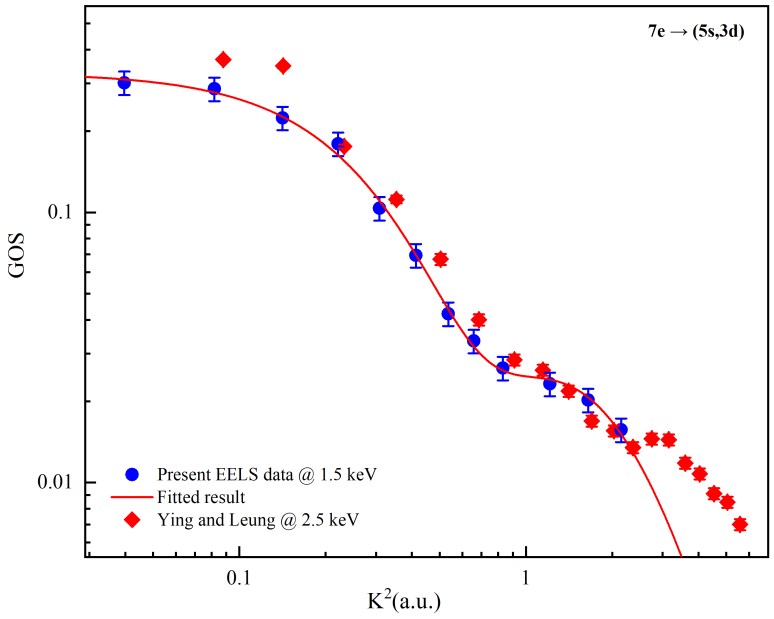


Figure 6: Same as Fig. 2, but for the $7e \rightarrow 5s, 3d$ transition.

Table 2: OOSs of the valence-shell excitations of CF_3Cl. Note that the OOS values have been multiplied by 10^2. Numbers in the parentheses are the experimental uncertainties.

Assignments	Energy	EELS	Photoabsorption			EELS	Dipole (e,e)	MR-CISD		EOM-CCSD
		Present	Ref. [10][a]	Ref. [14, 27]	Ref. [16, 27]	Ref. [19, 20]	Ref. [21][a]	Ref. [6]	Ref. [25, 26]	Ref. [27]
$7e \rightarrow 11a_1$	7.9	0.02(0.02)			0.02(0.01)	0.31(0.02)		1.1	0.27[25]	0.02
$7e \rightarrow 4s$	9.6	15.0(1.5)	17.5(3.5)	15.0(1.5)	14.5		15.0(0.7)	20.1	10.6[26]	16.0
$7e \rightarrow 4p$	10.6 10.9	12.3(1.3)	13.9(2.8)				12.2(0.6)			
$7e \rightarrow 5s, 3d$	11.5	33.0(3.0)	47.0(9.4)				27.0(1.3)			

[a]These data were extracted through fitting the spectra from Refs. [10, 21] with the same method employed in the present work.

The OOSs of the $7e \rightarrow (11a_1, 4s, 4p, (5s, 3d))$ transitions were determined through extrapolating the GOSs to $K^2 = 0$ with Lassettre formula (Eqs. (4) and (5)). Table 2 lists our OOS values along with the previous photoabsorption [10, 14, 16], EELS [19, 20] and dipole (e, e) [21] results. Note that the OOSs of Refs. [10, 21] were extracted through fitting their experimental data with the same method as adopted in the present study. The available theoretical OOSs [6, 25–27] are also listed in Table 2. Notably, Refs. [8, 9, 11–13, 15] reported the photoabsorption cross sections in limited wavelength regions, and the OOSs of Ref. [17] is much larger, so these data are not listed. It is clear in Table 2 that, except for the last transition, the present OOS values are in reasonable agreement with the data from Refs. [10, 14, 16, 21, 27] within the experimental uncertainties. However, we noticed that for the first transition the OOSs reported in Refs. [6, 19, 20, 25] are much higher than the present one. For the second transition, the OOS reported by Ref. [6] is higher while the one of Ref. [26] is lower compared with the present data. Regarding the last transition, the discrepancies between the present data and the previous measurements [10, 21] may be due to the contributions from higher-lying states and the corresponding fitting errors. Considering that our OOS values agree well with most previous results, especially for the strong dipole-allowed transition, we believe that the present results can serve as experimental benchmarks.

By performing integration on the GOS over the full range of K^2, the Born ICS can be obtained. However, the Born ICS may deviate from the true value where the FBA is invalid, i.e., at lower impact energies. To remedy this defect, Kim proposed the BE-scaling method [46, 47], which can scale the Born ICS to a more accurate value at low impact-energy region and keep its reliability at higher impact-energy region [45–48]. The BE-scaled ICS $\sigma_{BE}(E_0)$ is computed via

$$\sigma_{BE}(E_0) = \frac{E_0}{E_0 + B + E_n}\sigma_{Born}(E_0), \tag{6}$$

where E_0 denotes the incident electron energy, and B stands for the binding energy of the excited electron. The Born ICS $\sigma_{Born}(E_0)$ is calculated by

$$\sigma_{Born}(E_0) = \frac{\pi}{E_0 E_n}\int_{K^2_{min}}^{K^2_{max}} \frac{f(\mathbf{K}, E_n)}{K^2} dK^2. \tag{7}$$

Here, K^2_{min} and K^2_{max} stand for the squared momentum transfer calculated at $\theta = 0°$ and $\theta = 180°$, respectively.

According to Eqs. (6) and (7), the BE-scaled and Born ICSs of CF_3Cl were derived from the respective thresholds to 5000 eV, as displayed in Table 3 and Fig. 7. Since the BE-scaling method is valid solely on the premise that the transition is dipole-allowed, the Born ICS of the dipole-forbidden $7e \rightarrow 11a_1$ transition is given. In view of the large widths for all peaks, the calculated ICSs were convolved with the fitted peak profiles. It can be seen in Fig. 7 that the ICS data of all transitions have similar energy dependence, i.e., as the incident electron energy increases, the ICS curves gradually increase from the thresholds, and then decrease after reaching their maximum values. Among them, the Born ICS of $7e \rightarrow 11a_1$ rises more quickly and has a maximum at around 12 eV, whereas the BE-scaled ICSs of other transitions show slower increasing trends and exhibit the maxima at several tens of eV. As mentioned before, the Born ICS of $7e \rightarrow 11a_1$ may suffer from larger systematic errors in the low-energy region, while the remaining ICS data are generally of high reliability. Unfortunately, there are no other calculations or measurements available for comparison, and thus more investigations on the ICSs of the valence-shell excitations of CF_3Cl are highly recommended. All the datasets presented in this paper, including the GOSs, OOSs and ICSs, are compiled in the Supplementary Materials (SM) in PDF format.

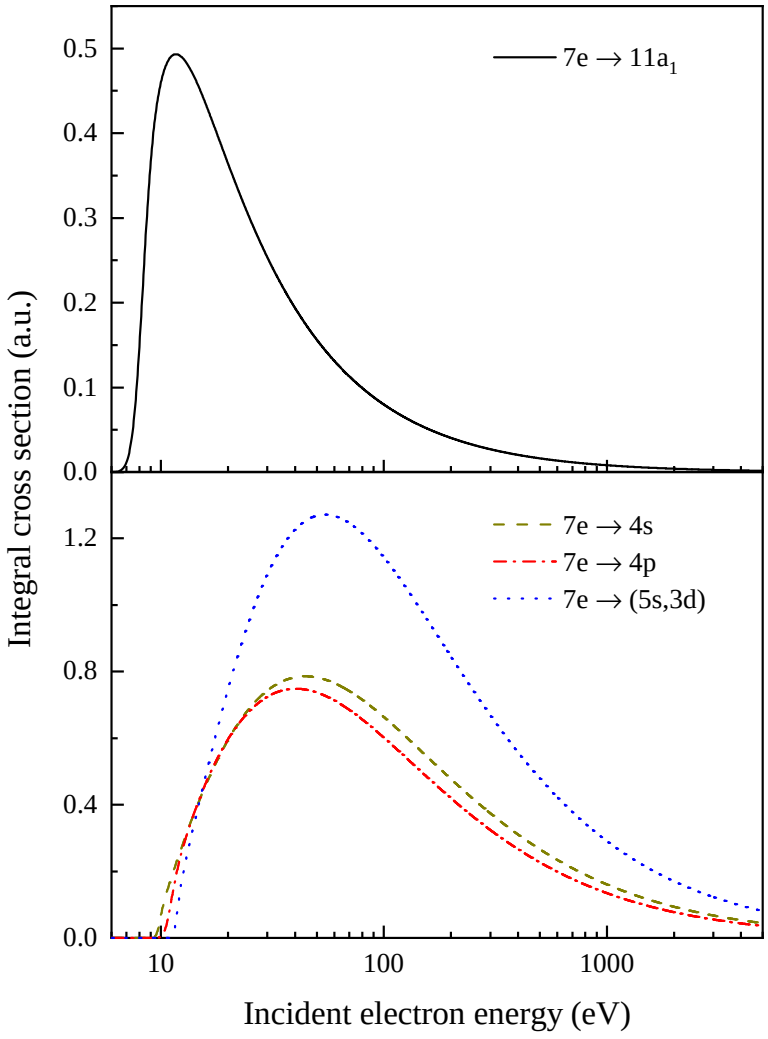


Figure 7: The Born ICS for the dipole-forbidden transition $7e \rightarrow 11a_1$ and the BE-scaled ICSs for the dipole-allowed transitions $7e \rightarrow (4s, 4p, (5s, 3d))$ of CF_3Cl at different incident electron energies.

Table 3: The present Born ICS (a.u.) for $7e \rightarrow 11a_1$ and BE-scaled ICSs (a.u.) for $7e \rightarrow 4s$, $7e \rightarrow 4p$ and $7e \rightarrow 5s, 3d$. The ICS values have been multiplied by 10^3, and the uncertainties are estimated to be approximately 20%.

E_0(eV)	$7e \rightarrow 11a_1$	$7e \rightarrow 4s$	$7e \rightarrow 4p$	$7e \rightarrow 5s, 3d$
6.5	1.17			
7	11.5			
7.5	53.7			
8	147.8			
8.5	268.6			
9	366.7	0.04		
9.5	426.5	8.65	0.34	
10	460.3	68.6	5.05	
12	492.5	246.5	221.9	109.3
16	432.2	464.1	470.2	497.3
20	364.0	595.0	596.9	747.9
30	253.5	743.2	724.4	1093.0
40	193.4	783.0	748.4	1226.9
50	156.3	782.4	737.3	1268.4
60	131.1	765.3	713.2	1267.2
70	113.0	741.4	684.9	1245.6
80	99.2	715.3	656.0	1214.4
90	88.5	689.0	627.9	1179.1
100	79.8	663.4	601.4	1142.4
200	40.4	477.0	419.3	844.1
400	20.4	310.4	266.4	556.7
600	13.7	234.2	198.7	422.1
800	10.3	189.9	159.9	343.1
1000	8.23	160.7	134.6	290.7
2000	4.14	93.6	77.4	170.0
3000	2.77	67.5	55.4	122.8
4000	2.08	53.3	43.6	97.0
5000	1.67	44.3	36.1	80.7

4. Summary and Conclusion

In this work, using a high-resolution EEL spectrometer, the GOSs for the valence-shell excitations $7e \rightarrow (11a_1, 4s, 4p, (5s, 3d))$ of CF_3Cl were measured at an incident electron energy of 1500 eV and an energy resolution of approximately 120 meV. The high resolution reduces the uncertainties stemmed from the random intensity allocations in the fitting procedure. Using the Lassettre formula, the GOSs were fitted and extrapolated to $K^2 = 0$ to determine the corresponding OOSs, which were used to cross-check the previous photoabsorption results, dipole (e,e) measurements and theoretical calculations. In addition, with the aid of the BE-scaling method, the Born ICS of $7e \rightarrow 11a_1$ and BE-scaled ICSs of $7e \rightarrow (4s, 4p, (5s, 3d))$ of CF_3Cl were calculated systematically from the corresponding thresholds up to 5000 eV. The data reported in this work serve to expand the fundamental molecular database of CF_3Cl and facilitate the relevant modeling research in atmospheric physics and plasma etching.

Acknowledgment

This work is supported by the National Natural Science Foundation of China (Grant No. 12334010) and the National Key Research and Development Program of China (Grant No. 2022YFA1602500). J.-F. Chen would also like to acknowledge the financial support from the Fundamental Research Funds for the Central Universities (Grant No. WK2030250112).

References

[1] Albright L F and Martin J J 1952 *Ind. Eng. Chem.* **44** 188–198 URL https://doi.org/10.1021/ie50505a053

[2] Tanaka H and Inokuti M 2000 *Adv. At. Mol. Opt. Phys.* **43** 1–17 URL https://doi.org/10.1016/S1049-250X(08)60120-2

[3] Martín I, Mayor E and Velasco A M 2006 *Theor. Chem. Acc.* **116** 614–620 URL https://doi.org/10.1007/s00214-006-0107-3

[4] Vollmer M K, Young D, Trudinger C M, Mühle J, Henne S, Rigby M, Park S, Li S, Guillevic M, Mitrevski B *et al.* 2018 *Atmos. Chem. Phys.* **18** 979–1002 URL https://doi.org/10.5194/acp-18-979-2018

[5] Chen J F and Zhu L F 2024 *Acta Phys. Sin.* **73** 095201 URL https://wulixb.iphy.ac.cn/cn/article/doi/10.7498/aps.73.20231598

[6] de Medeiros V C, de Andrade R B, Rodrigues G P, Bauerfeldt G F, Ventura E, Barbatti M and do Monte S A 2018 *J. Chem. Theory Comput.* **14** 4844–4855 URL https://doi.org/10.1021/acs.jctc.8b00457

[7] Montzka S A 2011 Source gases that affect stratospheric ozone *Stratospheric Ozone Depletion and Climate Change* ed Muller R (The Royal Society of Chemistry) URL https://doi.org/10.1039/9781849733182-00033

[8] Doucet J, Sauvageau P and Sandorfy C 1973 *J. Chem. Phys.* **58** 3708–3716 URL http://dx.doi.org/10.1063/1.1679722

[9] Gilbert R, Sauvageau P and Sandorfy C 1974 *J. Chem. Phys.* **60** 4820–4824 URL http://dx.doi.org/10.1063/1.1680987

[10] Jochims H W, Lohr W and Baumgärtel H 1976 *Ber. Bunsen-Ges. Phys. Chem.* **80** 130–138 URL https://doi.org/10.1002/bbpc.19760800208

[11] Lee L C, Phillips E and Judge D L 1977 *J. Chem. Phys.* **67** 1237–1246 URL http://dx.doi.org/10.1063/1.434935

[12] Hubrich C and Stuhl F 1980 *J. Photochem.* **12** 93–107 URL https://doi.org/10.1016/0047-2670(80)85031-3

[13] Washida N, Suto M, Nagase S, Nagashima U and Morokuma K 1983 *J. Chem. Phys.* **78** 1025–1032 URL http://dx.doi.org/10.1063/1.444902

[14] Suto M and Lee L C 1983 *J. Chem. Phys.* **79** 1127–1133 URL http://dx.doi.org/10.1063/1.445914

[15] Simon P C, Gillotay D, Vanlaethem-Meuree N and Wisemberg J 1988 *J. Atmos. Chem.* **7** 107–135 URL https://doi.org/10.1007/BF00048042

[16] Eden S, Limão-Vieira P, Hoffmann S V and Mason N J 2006 *Chem. Phys.* **323** 313–333 URL https://doi.org/10.1016/j.chemphys.2005.09.040

[17] King G C and McConkey J W 1978 *J. Phys. B: Atom. Mol. Phys.* **11** 1861 URL http://doi.org/10.1088/0022-3700/11/10/020

[18] Zhang W, Cooper G, Ibuki T and Brion C E 1991 *Chem. Phys.* **151** 343–356 URL https://doi.org/10.1016/0301-0104(91)80020-I

[19] Ying J F and Leung K T 1994 *J. Chem. Phys.* **101** 8333–8350 URL http://dx.doi.org/10.1063/1.468098

[20] Ying J F, Mathers C P, Leung K T, Pritchard H P, Winstead C and McKoy V 1993 *Chem. Phys. Lett.* **212** 289–297 URL https://doi.org/10.1016/0009-2614(93)89328-F

[21] Au J W, Burton G R and Brion C E 1997 *Chem. Phys.* **221** 151–168 URL https://doi.org/10.1016/S0301-0104(97)00146-8

[22] Velasco A M, Mayor E and Martín I 2003 *Chem. Phys. Lett.* **377** 189–196 URL https://doi.org/10.1016/S0009-2614(03)01132-1

[23] Mayor E, Velasco A M and Martín I 2005 *Chem. Phys. Lett.* **404** 35–39 URL https://doi.org/10.1016/j.cplett.2005.01.028

[24] Pitarch-Ruiz J, Sánchez de Merás A, Sánchez-Marín J, Mayor E, Velasco A M and Martín I 2007 *J. Phys. Chem. A* **111** 3321–3325 URL https://doi.org/10.1021/jp070210z

[25] Jr Lucena J R, Ventura E, do Monte S A, Araújo R C M U, Ramos M N and Fausto R 2007 *J. Chem. Phys.* **127** 164320 URL https://doi.org/10.1063/1.2800020

[26] de Medeiros V C, Ventura E and do Monte S A 2012 *Chem. Phys. Lett.* **546** 30–33 URL https://doi.org/10.1016/j.cplett.2012.07.037

[27] Watanabe N and Takahashi M 2022 *J. Phys. B: At. Mol. Opt. Phys.* **55** 015201 URL https://doi.org/10.1088/1361-6455/ac4a22

[28] Sun Q, Wang S X, Xu Y C, Ma K, Wang L H, Li T J and Zhu L F 2022 *J. Electron Spectrosc. Relat. Phenom.* **258** 147218 URL https://doi.org/10.1016/j.elspec.2022.147218

[29] Wang D H, Wang S X, Nie Z W, Wang L H, Xu Y C, Du X J and Zhu L F 2022 *Plasma Sources Sci. Technol.* **31** 045012 URL https://doi.org/10.1088/1361-6595/ac5e51

[30] Wang L H, Du X J, Xu Y C, Nie Z W, Wang D H, Wang S X and Zhu L F 2022 *J. Phys. Chem. A* **126** 453–461 URL https://doi.org/10.1021/acs.jpca.1c10171

[31] Bilal M M, Chen J F, Nie Z W, Zhu J H and Zhu L F 2025 *Eur. Phys. J. D* **79** 33 URL https://doi.org/10.1140/epjd/s10053-025-00979-y

[32] Wu S L, Zhong Z P, Feng R F, Xing S L, Yang B X and Xu K Z 1995 *Phys. Rev. A* **51**(6) 4494–4500 URL https://doi.org/10.1103/PhysRevA.51.4494

[33] Xu K Z, Feng R F, Wu S L, Ji Q, Zhang X J, Zhong Z P and Zheng Y 1996 *Phys. Rev. A* **53**(5) 3081–3086 URL https://doi.org/10.1103/PhysRevA.53.3081

[34] Liu X J, Zhu L F, Jiang X M, Yuan Z S, Cai B, Chen X J and Xu K Z 2001 *Rev. Sci. Instrum.* **72** 3357–3361 URL http://dx.doi.org/10.1063/1.1382636

[35] Khakoo M A and Trajmar S 1986 *Phys. Rev. A* **34**(1) 138–145 URL https://doi.org/10.1103/PhysRevA.34.138

[36] Nickel J C, Zetner P W, Shen G and Trajmar S 1989 *J. Phys. E: Sci. Instrum.* **22** 730–738 URL https://doi.org/10.1088/0022-3735/22/9/010

[37] Liu Y W, Xu L Q, Ni D D, Xu X, Huang X C and Zhu L F 2017 *J. Geophys. Res. Space Phys.* **122** 3459–3468 URL https://doi.org/10.1002/2016JA023857

[38] Zhong Z P, Feng R F, Xu K Z, Wu S L, Zhu L F, Zhang X J, Ji Q and Shi Q C 1997 *Phys. Rev. A* **55** 1799 URL https://doi.org/10.1103/PhysRevA.55.1799

[39] Inokuti M 1971 *Rev. Mod. Phys.* **43**(3) 297–347 URL https://doi.org/10.1103/RevModPhys.43.297

[40] Cann N M and Thakkar A J 2002 *J. Electron Spectrosc. Relat. Phenom.* **123** 143–159 URL https://doi.org/10.1016/S0368-2048(02)00016-6

[41] Han X Y and Li J M 2006 *Phys. Rev. A* **74** 062711 URL https://doi.org/10.1103/PhysRevA.74.062711

[42] Xie B P, Zhu L F, Yang K, Zhou B, Hiraoka N, Cai Y Q, Yao Y, Wu C Q, Wang E L and Feng D L 2010 *Phys. Rev. A* **82** 032501 URL https://doi.org/10.1103/PhysRevA.82.032501

[43] Lassettre E N 1965 *J. Chem. Phys.* **43** 4479–4486 URL http://dx.doi.org/10.1063/1.1696720

[44] Vriens L 1967 *Phys. Rev.* **160**(1) 100–108 URL https://doi.org/10.1103/PhysRev.160.100

[45] Tanaka H, Brunger M J, Campbell L, Kato H, Hoshino M and Rau A R P 2016 *Rev. Mod. Phys.* **88** 025004 URL https://doi.org/10.1103/RevModPhys.88.025004

[46] Kim Y K 2001 *Phys. Rev. A* **64**(3) 032713 URL https://doi.org/10.1103/PhysRevA.64.032713

[47] Kim Y K 2007 *J. Chem. Phys.* **126** 064305 URL http://dx.doi.org/10.1063/1.2434163

[48] Wang S X and Zhu L F 2022 *Chin. Phys. B* **31** 083401 URL https://doi.org/10.1088/1674-1056/ac6336